RSC Advances

ROYAL SOCIETY OF CHEMISTRY

www.rsc.org/advances

Tailoring Self-assembly Behavior of Biological Surfactant By Imidazolium-based Surfactants with Different Length of Hydrophobic Alkyl Tails

Zhaohua Song [a], Xia Xin [a, b*], Jinglin Shen [b], Han Zhang [b], Shubin Wang [b], Yanzhao Yang [a *]

[a] *National Engineering Technology Research Center for Colloidal Materials, Shandong University, Shanda nanlu No. 27, Jinan, 250100, P. R. China*

[b] *Key Laboratory of Colloid and Interface Chemistry (Shandong University), Ministry of Education, Shanda nanlu No. 27, Jinan, 250100, P. R. China*

[*] Author to whom correspondence should be addressed, E-mail: xinx@sdu.edu.cn.

Phone: +86-531-88363597. Fax: +86-531-88361008

[*] Author to whom correspondence should be addressed, E-mail: yzhyang@sdu.edu.cn.

Phone: +86-531-88362988. Fax: +86-531-88361008

Abstracts

In this work, the effects of four imidazolium-based surfactants with different length of hydrophobic alkyl tails ([C_2mim]Br, [C_8mim]Br, [C_{12}mim]Br, and [C_{14}mim]Br) on the self-assembly behaviors of biological surfactant sodium deoxycholate (NaDC) in sodium phosphate buffer (pH = 7) were investigated systematically. The microstructures and properties of NaDC/$C_n$mimBr (n=2, 8, 12, 14) mixed systems were characterized using transmission electron microscopy (TEM), field emission-scanning electron microscopy (FE-SEM), polarized optical microscopy (POM) observations, Fourier transform infrared (FT-IR), X-ray powder diffraction (XRD) and rheological measurements. The roles of the hydrophobic chain length, the chiral rigid steroid center, and the electrostatic interaction for the evolution of phase behavior are clearly described. The results indicated that the long-chain imidazolium-based surfactants ([$C_n$mim]Br, n≥8) weakened the gel of NaDC, while C_2mimBr strengthened the gel behavior of NaDC and even can form microcrystals. The superhydrogels formed by these systems may be act as promising adsorbents for the removal of heavy-metal ions from industrial sewage.

Keywords: Biological surfactant; Imidazolium-based surfactant; Hydrogels; Microcrystals;

Introduction

The concept of self-assembly is that small structural units, such as atoms, molecules, macroions, or nanoclusters self-organize into more complicated functional supramolecular structures with well-defined shapes, sizes, and properties which can avoid complex organic synthesis [1-3]. They have attracted considerable interest for applications in drug delivery, tissue engineering, catalysis, electronics, photonics, light-energy conversion, etc [4-6]. The supramolecular structures can be self-assembled via weak non-covalent interactions by several strategies such as hydrogen bonding, electrostatic interaction, hydrophobic interaction, van der Waals interaction, metal coordination, and π-conjugation [7-9].

Among them, specifically, ionic self-assembly (ISA) which is the most powerful tool on the basis of electrostatic interactions has initiated extensive research due to its advantages of generalizability, simplicity, cheapness, and flexibility [10-12]. For example, Wang et al. [13] revealed that robust porphyrin nanotubes can be prepared by ionic self-assembly of two oppositely charged porphyrins in aqueous solution. The electrostatic forces between these porphyrin tectons, in addition to the van der Waals, hydrogen bonding, axial coordination, and other weak intermolecular interactions that typically contribute to the formation of porphyrin aggregates, enhance the structural stability of these nanostructures. Zhang et al. [14] facilely organized the inorganic sandwiched heteropolytungstomolybdate $K_{13}[Eu(SiW_9Mo_2O_{39})_2]$ (E) into highly ordered supramolecular nanostructured materials by complexation with a series of cationic surfactants achieved by ISA route and it is demonstrated that the amphiphilic cationic surfactants not only play a structural role but also have a strong influence on the photophysical properties of E. Gong et al. [15] employed an ISA strategy to fabricate pH and temperature responsive supramolecular materials

with controllable fluorescence emission properties by using charged Congo red (CR) and an oppositely charged COOH-functionalized imidazolium-based surface active ionic liquid (SAIL), N-decyl-N′-carboxymethyl imidazolium bromide ([N-C_{10}, N′-COOH-Im]Br).

SAILs, referred to as the ionic liquids containing long alkyl chains have emerged as a novel kind of amphiphiles which can exhibit amphiphilic character [16-18]. Moreover, it is also demonstrated that compared to the traditional surfactants, they usually display superior surface-active properties and specific phase behavior in aqueous media. Among them, imidazolium-based surfactant is one kinds of surface active ionic liquids. Besides, unlike the typical surfactant which presents a polar head and a nonpolar tail, the bile salt possesses a rigid steroid backbone which has polar hydroxyl groups on the concave α-face and methyl groups on the convex β-face [19-21]. Thus, bile salts can be regarded as an unusual class of amphiphiles. Among them, sodium deoxycholate (NaDC) is one kinds of biocompatible, biodegradable, and nontoxic bile salt [22-24]. Herein, in this article, we successfully investigated the phase behavior and the physicochemical properties of the complex formed with long-chain imidazolium-based surfactants ([$C_n$mim]Br) and biological surfactant NaDC through ISA route by operating transmission electron microscopy (TEM), field emission-scanning electron microscopy (FE-SEM), polarized optical microscopy (POM) observations, Fourier transform infrared (FT-IR), X-ray powder diffraction (XRD) and rheological measurements. This research is an extension of the work of interaction between NaDC and different kind of materials in our laboratory and it provides another example to assemble different structures using ISA strategy.

Experimental methods

Chemicals and Materials.

Sodium deoxycholate (NaDC, A.R.), NaH_2PO_4 and Na_2HPO_4 (A.R.) were purchased from Sinopharm Chemical Reagent Co. Long-chain imidazolium-based surfactants ([C_2mim]Br, [C_8mim]Br, [C_{12}mim]Br, and [C_{14}mim]Br) was purchased from Lanzhou institute of chemical physics with the purity greater than 99%. Ultrapure water with a resistivity of 18.25 MΩ cm was obtained using a UPH-IV ultrapure water purifier (China).
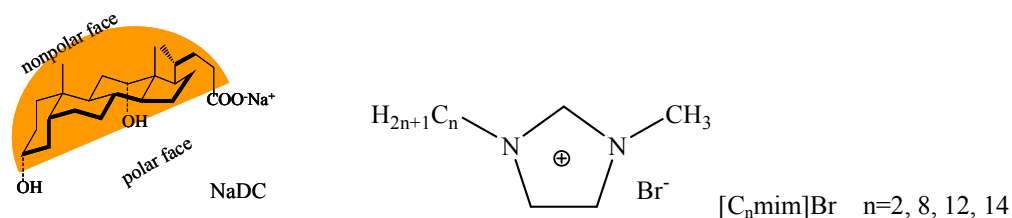
Figure 1 The structures of NaDC and cationic imidazolium-based surfactants

Sample Preparation (Phase behavior observation)

It is important to remark that the pKa of the carboxylic group of bile acids depends on the local environment, and it is sensitively higher in the aggregates than in the free molecule [25]. Thus, all solutions were prepared in sodium phosphate buffer with pH = 7 (100 mmol L^{-1}), which was prepared by mixing desired amounts of NaH_2PO_4 and Na_2HPO_4 in water, to control the pH of the samples. Thus, samples were prepared by mixing aqueous solutions of NaDC and [$C_n$mim]Br at certain concentration in PBS buffer solutions to the final total volume of 3 mL. The solutions were gently stirred to accelerate the dissolution process. Then the samples were equilibrated at 20.0 ± 0.1 °C for at least 4 weeks before the phase behavior was inspected. Phase behavior was studied by visual inspection.

Methods and Characterization

For transmission electron microscopy (TEM) observations, ~5 μ L of solution was placed on a copper grid and the excess solution was wicked away by a piece of filter paper. After drying, the

copper grid was checked by a JEOL JEM-100 CXII (Japan) at an accelerating voltage of 80 kV. For field-emission scanning electron microscopy (FE-SEM) observations, a drop of hydrogel was placed on a silica wafer to form a thin film, which was then freeze-dried in vacuum at $-55°C$. A layer of gold was sputtered on top to make the conducting surface. The wafer was observed on a JSM-6700F FE-SEM. Fourier transform infrared (FTIR) spectrum was recorded on a VERTEX-70/70v spectrometer (Bruker Optics, Germany). XRD patterns were obtained on a Rigaku D/Max 2200-PC diffractometer with Cu Ka radiation ($\lambda = 0.15418$ nm) and a graphite monochromator. Data (2θ) were collected from $10°$ to $70°$. The samples prepared for FTIR and XRD were all frozen in a vacuum extractor at -55°C for 1 day. Polarized optical microscopy observations were performed using an AXIOSKOP 40/40 FL (ZEISS,Germany) microscope. The right amount of samples were dropped into a 1 mm thick trough, and then were covered by cover glass to avoid solvent evaporation.

The rheological measurements were carried out on a HAAKE RS75 rheometer with a cone-plate system (Ti, diameter, 35 mm; cone angle, $1°$). For the shear-dependent behavior, the viscosity measurements were carried out at shear rates ranging from 0 to 1000 s^{-1}. In oscillatory measurements, an amplitude sweep at a fixed frequency of 1 Hz was performed prior to the following frequency sweep in order to ensure that the selected stress was in the linear viscoelastic region. The viscoelastic properties of the samples were determined by oscillatory measurements in the frequency range of 0.01-10 Hz. The samples were measured at 20.0 ± 0.1 °C with the help of a cyclic water bath.

Results and Discussion

Phase behavior of NaDC/$C_n$mimBr mixed systems

To understand how the phase transition influenced by using the ISA strategy, firstly, we observed the $[C_{14}mim]Br$/NaDC mixed system at different concentrations. The phase behavior of $[C_{14}mim]Br$/NaDC mixed system with the addition of $[C_{14}mim]Br$ to 50 mmol L^{-1} NaDC solutions and sample photographs of typical samples are shown in Figure 2. It can be seen that with the addition of $[C_{14}mim]Br$, the samples experienced the evolution of various phase behavior including hydrogel, sol, precipitate, two phase, solution and lyotropic liquid crystal (LLC) phases. It can be inferred that the evolution of rich phase behavior could be a result of the balance between different interaction such as electrostatic interaction, hydrophobic interaction and hydrogen bond interaction [26, 27]. Especially, when the concentration of $[C_{14}mim]Br$ increase, the electrostatic interaction between NaDC and $[C_{14}mim]Br$ is the main driving force. The stronger electrostatic interactions between the headgroup of $[C_{14}mim]Br$ and NaDC destroy the hydrogel state of NaDC and changed to other states. Moreover, for comparation, the samples without sodium phosphate buffer were prepared and shown in Figure S1. It can be concluded that the PBS as a kind of salts is benefical to the gelation [28].
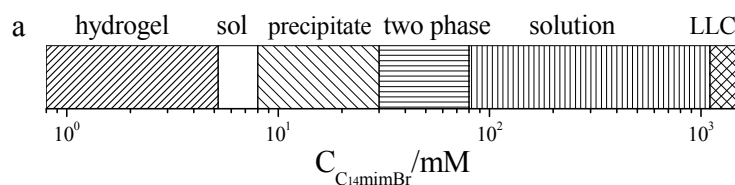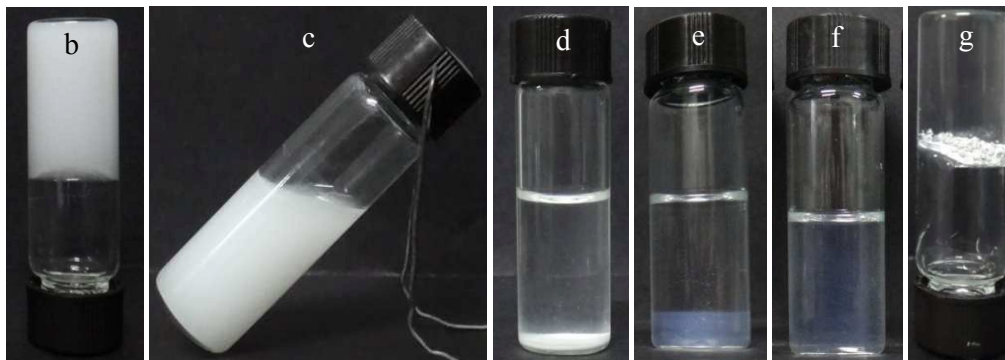
Figure 2 (a) Phase transition with the addition of [C$_{14}$mim]Br to 50 mmol L^{-1} NaDC samples and

the photographs of typical samples : c_{NaDC} = 50 mmol L^{-1} and $c_{[C14mim]Br}$ is changeable: (b) 5, (c) 7.5,

(d) 20, (e) 75, (f) 100, (g) 1500 mmol L^{-1}. T = 20.0 ± 0.1℃. The concentration of sodium phosphate

buffer solutions (pH = 7) in all samples are fixed at 100 mmol L^{-1}.

Furthermore, it is well-known that hydrophobic effect will be greatly influenced by the

surfactant chain length [29-31]. Thus, in order to explore the role of hydrophobic interaction

provided by the hydrophobic chain of SAIL on the effect of phase transition and the formation of

self-assembly structures, the hydrophobic chain length of SAIL was changed and [C$_2$mim]Br,

[C$_8$mim]Br and [C$_{12}$mim]Br were selected for comparison. The phase behaviors of [C$_n$mim]Br (n =

2, 8, 12, 14)/NaDC mixed systems are shown in Figure 3. It can be seen that [C$_{14}$mim]Br can

induce the evolution of phase behavior at the low concentration and next is [C$_{12}$mim]Br and

[C$_8$mim]Br. If the hydrophobic chains are too short (such as [C$_2$mim]Br), the phase behavior is not

rich and it can not destroy the hydrogel state of NaDC even when its concentration reached at 1200

mmol L^{-1}.These phenomena prove that only appropriate hydrophobic interactions can contribute to

the rich changes in phase behavior. An increase in the hydrophobic chain length (n changed from 8

to 14) can result in the enhancement of the hydrophobic interaction. Consequently, the aggregates

formed by NaDC and [C$_n$mim]Br tend to grow to reduce the chain's contact area with water [32]. If

the hydrophobic chains are too short ([C$_2$mim]Br), the hydrophobic effect is not strong enough to

influence the self-assemble behavior of NaDC. Therefore, it can be concluded that in our systems,

besides the main electrostatic interaction, the appropriate hydrophobic chain length of [C$_n$mim]Br

plays a crucial role in the modification of effective molecular stacking and the formation of

different self-assembly structures.

Figure 3 Phase behavior of [C$_n$mim]Br (n = 2, 8, 12, 14)/NaDC mixed systems after equilibrated at

20.0 ± 0.1 ºC for at least 4 weeks. The concentration of NaDC is fixed at 50 mmol L^{-1} and the

concentrations of [C$_n$mim]Br is from 1 to 1500 mmol L^{-1}. ■: hydrogel; ●: sol; ▲: precipitate;

▼:two phase; ◄: solution; ►: LLC.

Observation of morphology transitions

The various morphologies of the superstructures for different phases created in the

[C$_n$mim]Br/NaDC mixed systems were examined using TEM. Firstly, TEM results of

[C$_{14}$mim]Br/NaDC mixed system with the addition of different concentration of [C$_{14}$mim]Br to 50

mmol L^{-1} NaDC samples were investigated. It can be seen that the sample of 50 mmol L^{-1} NaDC

has a network structure and after the addition of [C$_{14}$mim]Br, the network can be destroyed

gradually. When the concentration of [C$_{14}$mim]Br ($c_{[C14mim]Br}$) reached at 7.5 mmol L^{-1}, the hydrogel

changed to sol state and the spherical aggregates exist in the system. With further addition of

[C$_{14}$mim]Br ($c_{[C14mim]Br}$ = 10 mmol L^{-1}), it changed to two phase state and the upper solution phase

is network and the bottom phase is irregular shape of massive precipitation. When $c_{[C14mim]Br}$ = 75

mmol L^{-1}, the morphology of the upper phase is micelle and the bottom phase (light blue) is vesicle.

When $c_{[C14mim]Br}$ = 100 mmol L^{-1}, the whole light blue phase is vesicle. Scheme 1 illustrates the

possible mechanism of vesicles formed with the addition of 100 mM [C$_{14}$mim]Br into 50 mM
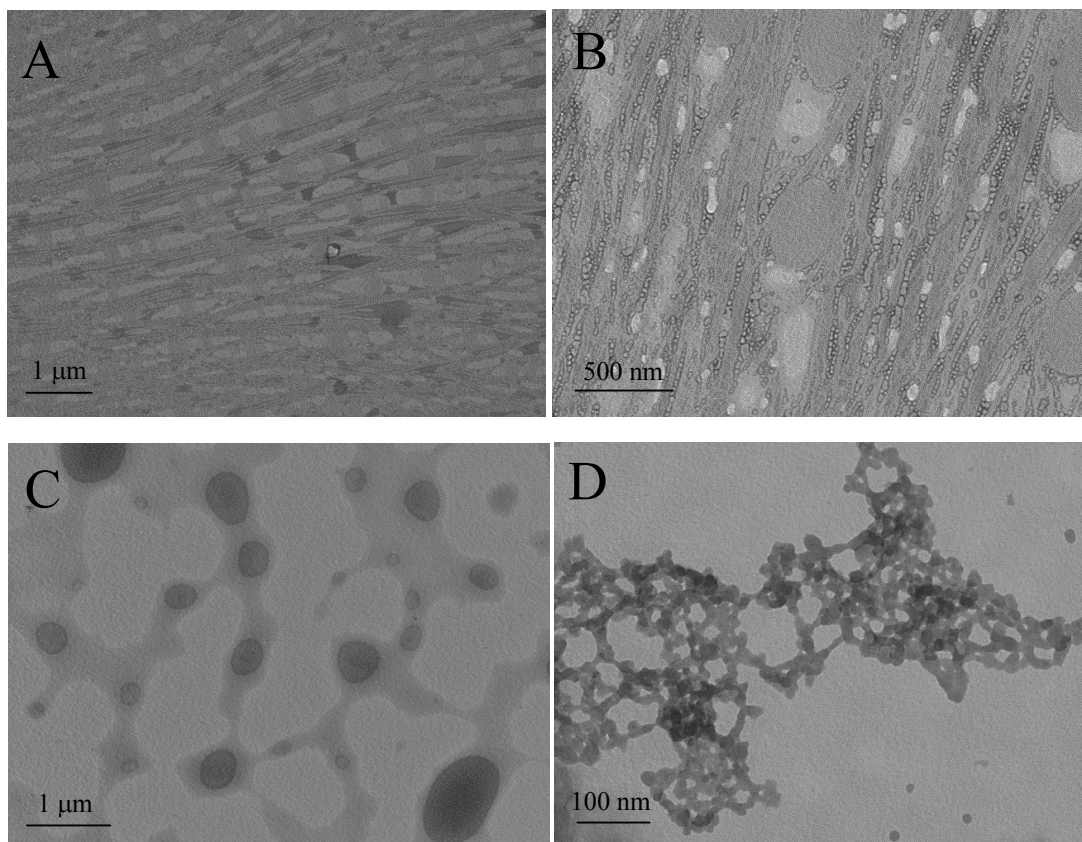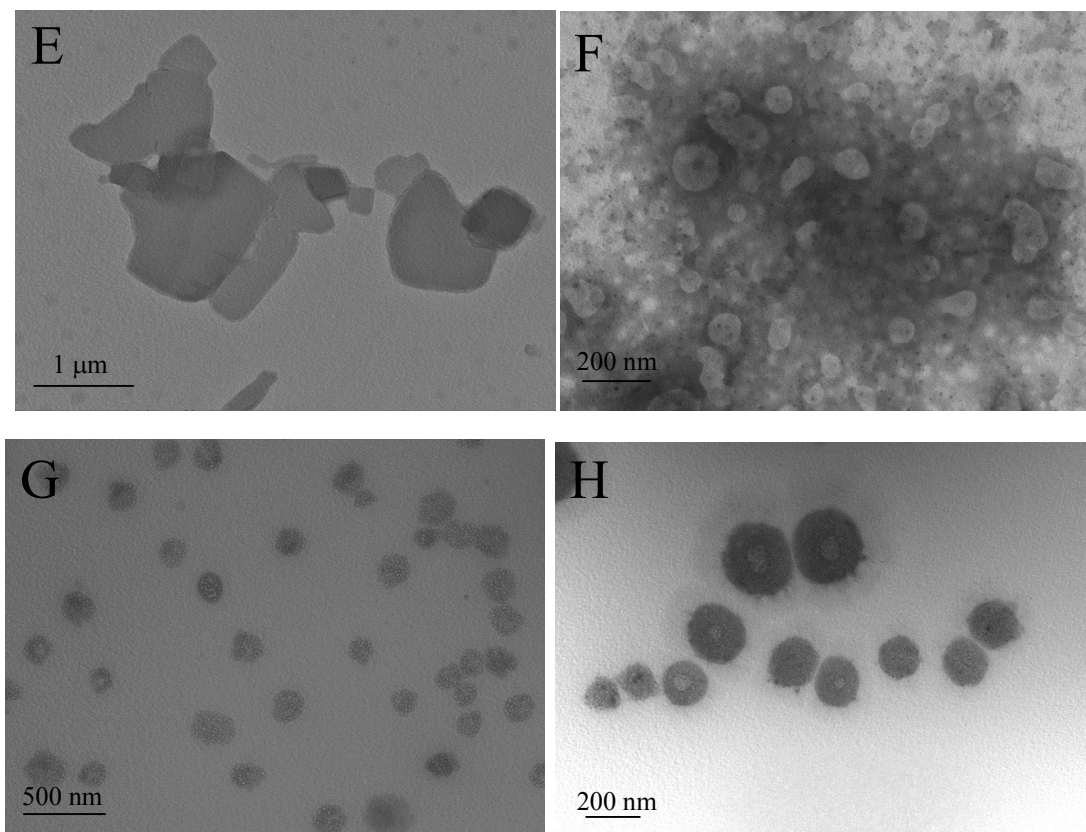
NaDC.

Figure 4 TEM results of [C$_{14}$mim]Br/NaDC mixed system with the addition of different concentration of [C$_{14}$mim]Br to 50 mmol L^{-1} NaDC solutions. (A) 0 mmol L^{-1} (hydrogel); (B) 5 mmol L^{-1} (hydrogel); (C) 7.5 mmol L^{-1} (sol); (D) 10 mmol L^{-1} (the upper phase: solution); (E) 10 mmol L^{-1} (the bottom phase: precipitate); (F) 75 mmol L^{-1} (the upper phase: solution) (G) 75 mmol L^{-1} (the bottom phase: solution); (H) 100 mmol L^{-1} (solution).

Secondly, if we fixed the concentration of [C$_n$mim]Br (100 mmol L^{-1}) and varied the hydrophobic chain length (n changed from 2 to 14), they also have different morphologies because of the different states of the samples. TEM and SEM results of 100 mmol L^{-1} [C$_n$mim]Br/50 mmol L^{-1} NaDC mixed system are shown in Figure 5 and the photographs of typical samples are shown in Figure S2. It can be seen that with the decrease of hydrophobic chain length, it transformed from vesicle (n = 12, 14) to two phase (n = 8) and to hydrogel state (n = 2), respectively. Moreover, the

increase of the concentration of [C$_n$mim]Br has the same effect on the phase transition behavior compared with the increase of hydrophobic chain length of [C$_n$mim]Br, which proves again that besides the electrostatic interaction influences the phase behavior, the hydrophobic effect also greatly contributes to the self-assemble behavior. Overall, it can be deduced that the electrostatic attraction, hydrophobic effect, and geometric packing all influence the phase behavior and the self-assembly structures of NaDC/[C$_n$mim]Br mixed systems.
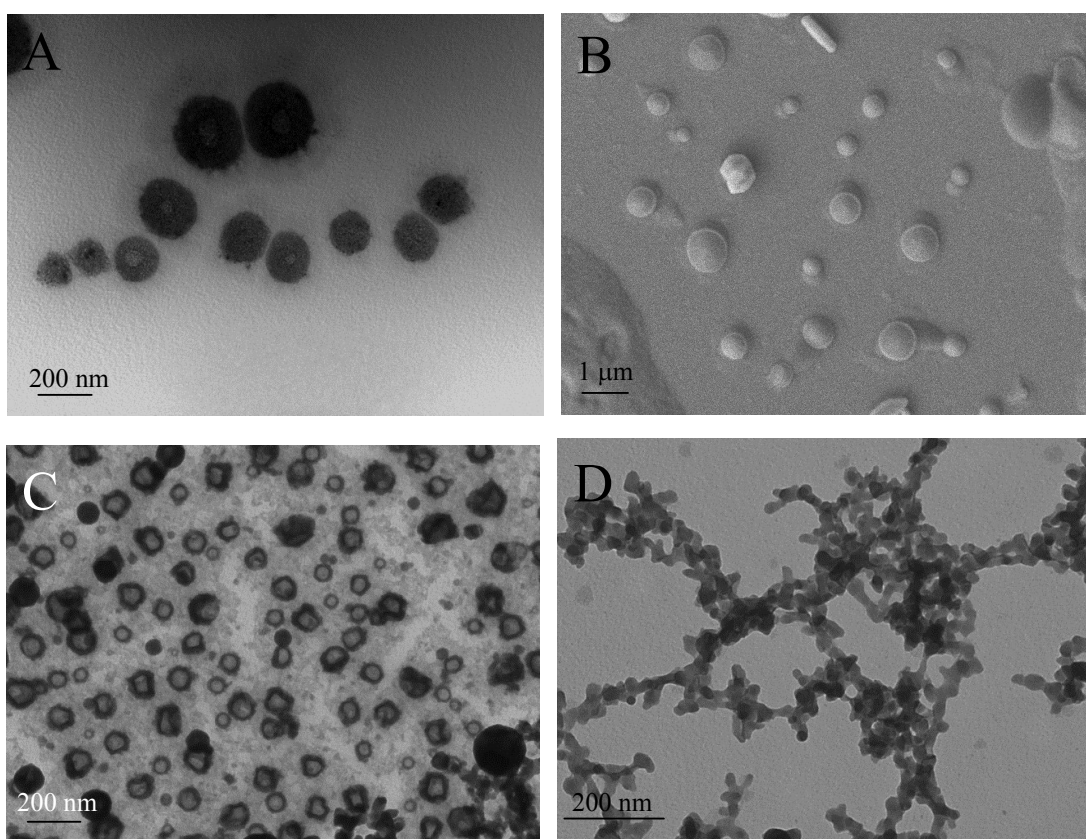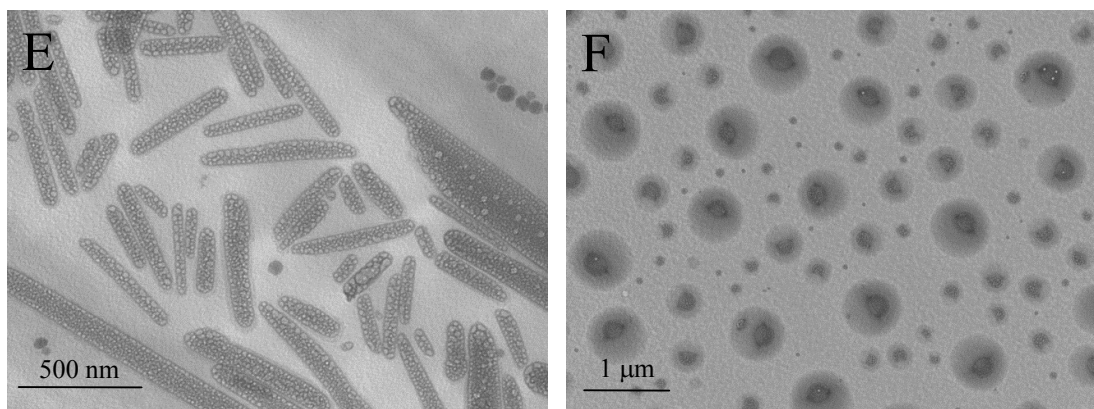
Figure 5 TEM and SEM results of 100 mmol L^{-1} [C$_n$mim]Br/50 mmol L^{-1}NaDC mixed system. TEM results: (A) [C$_{14}$mim]Br; (C) [C$_{12}$mim]Br; (D) [C$_8$mim]Br (the upper phase: solution); (E) [C$_8$mim]Br (the bottom phase: solution); (F) [C$_2$mim]Br. (B) SEM result for [C$_{14}$mim]Br.
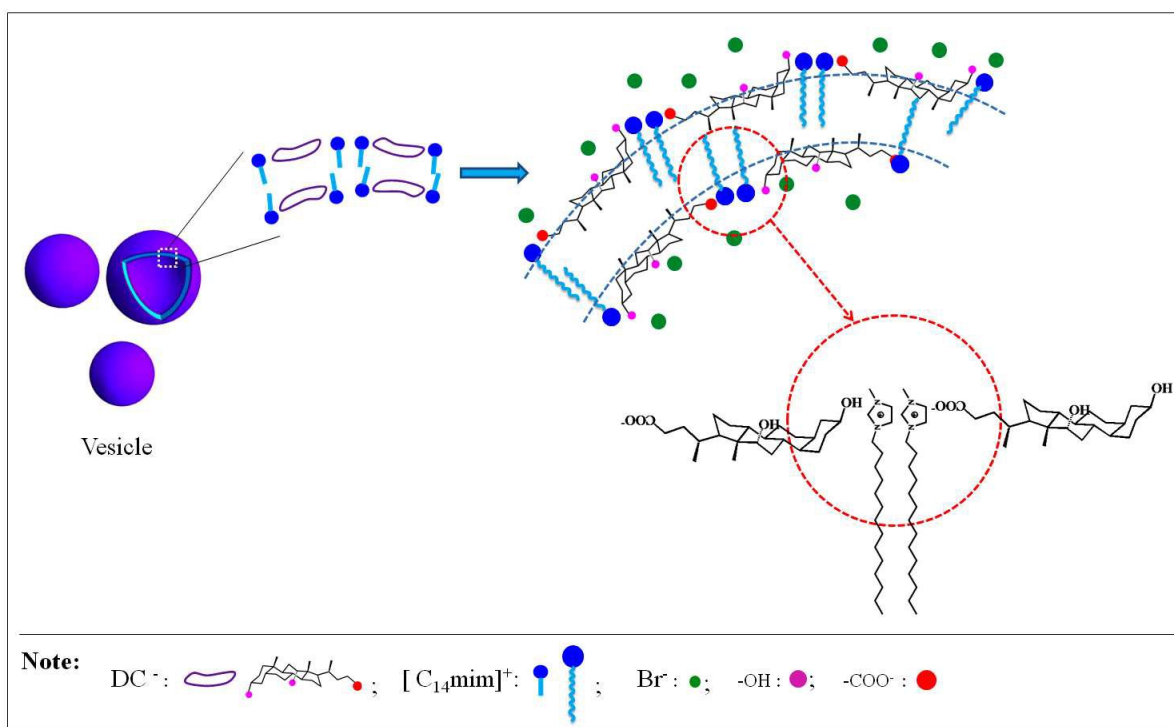
Scheme 1 The possible mechanism of vesicles formed with the addition of 100 mM [C$_{14}$mim]Br into 50 mM NaDC gels.

Rheological properties

Rheological behavior is one of the most important methods to characterize the viscoelasticity of hydrogels, by measuring the viscosity and elasticity of hydrogels [22]. The stress sweep test was executed at a fixed frequency of 1.0 Hz for [C$_{14}$mim]Br/NaDC mixed system with the addition of different concentration of [C$_{14}$mim]Br (0-7.5 mmol L^{-1}) to 50 mmol L^{-1} NaDC solutions. It can be seen that with the addition of more and more [C$_{14}$mim]Br, the G′ values and G″ values keep gradually decreasing. When $c_{[C14mim]Br}$ were below 5 mmol L^{-1}, G′ is higher than G″, while $c_{[C14mim]Br}$ = 5 mmol L^{-1}, the curves of G′ and G″ have a crossing point. After that, the system has the viscous dominant property. These results indicate that the structure of the hydrogel is destroyed, and the result is consistent with TEM observation.

Moreover, the dynamically rheological data of 5 mmol L^{-1} [C$_n$mim]Br (n changed from 2 to 14)/50 mmol L^{-1}NaDC mixed system are shown in Figure 7. It can be seen that with the same concentration of [C$_n$mim]Br (5 mmol L^{-1}), [C$_{14}$mim]Br can decrease the viscosity and elasticity of hydrogels the most heavily, the next is [C$_{12}$mim]Br and [C$_8$mim]Br is the minimum. This means that the longer the hydrophobic chain length, the higher the hydrophobic effect which can destroy the network structure of the hydrogels. For [C$_2$mim]Br, it not only did not reduce the viscosity and elasticity of hydrogel, but increased. This may be because that [C$_2$mim]Br is a small molecule and can act as a bridge to enhance the network structure because of the hydrogen bond interaction between NaDC and [C$_2$mim]Br.
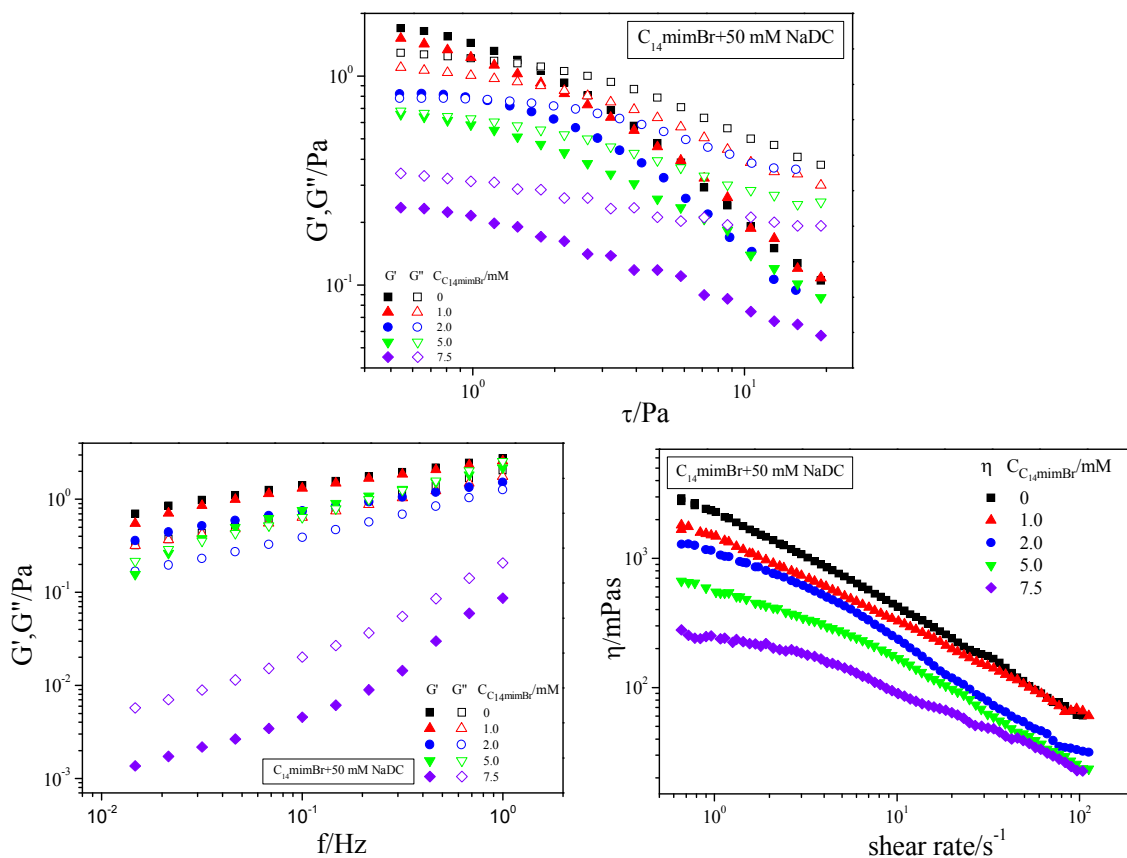
Figure 6 Dynamically rheological data of [C_{14}mim]Br/NaDC mixed system with the addition of different concentration of [C_{14}mim]Br to 50 mmol L^{-1} NaDC solutions (A) G' and G'' as a function of the applied stress at a constant frequency (1.0 Hz), (B) variation of G' and G'' as a function of frequency and (C) variation of shear viscosity as a function of shear rate.
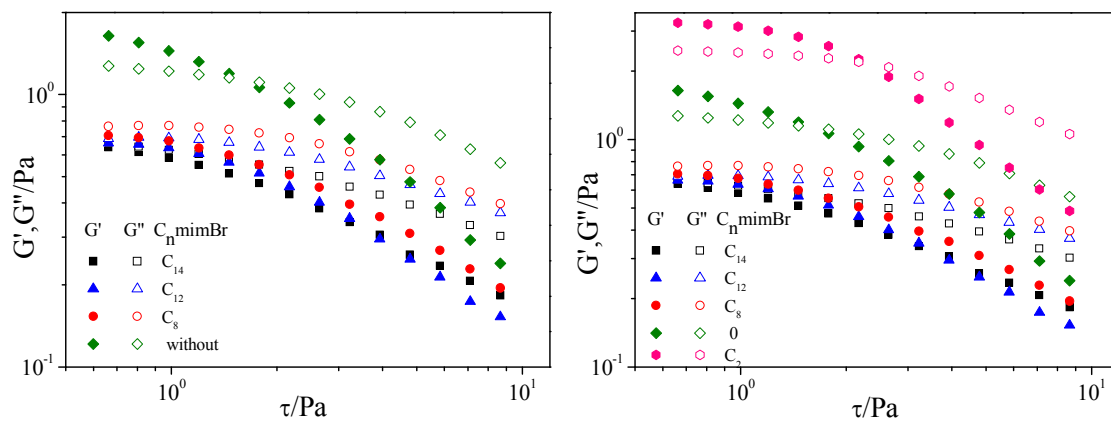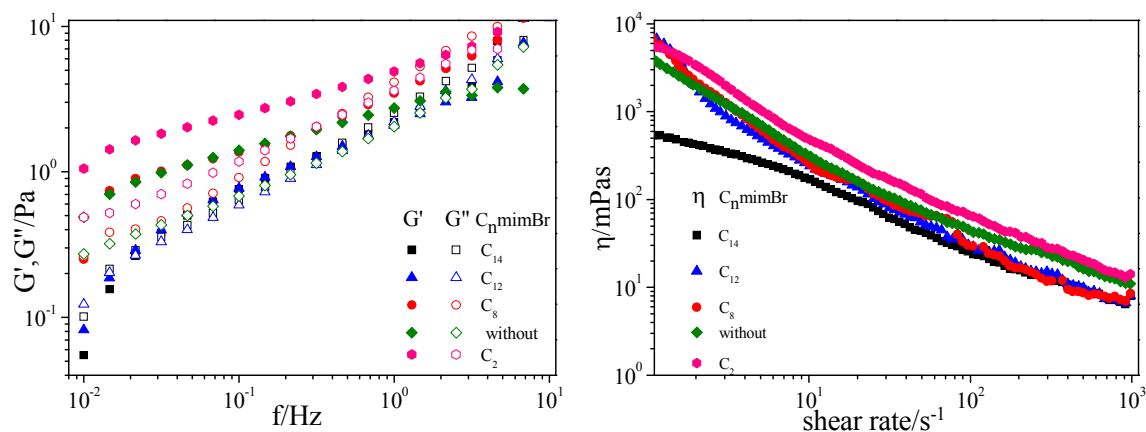
Figure 7 Dynamically rheological data of 5 mmol L^{-1} [C$_n$mim]Br/50 mmol L^{-1}NaDC mixed system. (A) G′ and G″ as a function of the applied stress at a constant frequency (1.0 Hz), (B) variation of G′ and G″ as a function of frequency and (C) variation of shear viscosity as a function of shear rate.

FT-IR and XRD analyses

FT-IR is an important method to characterize the interactions of self-assembling supramolecular hydrogels [33] and the results of our samples are shown in Figure 8. It is well-known that the frequencies for the antisymmetric v_{as}(CH$_2$) and the symmetric stretching v_s(CH$_2$) bands are sensitive to the conformation of the alkyl chains [15]. It can be seen that the v_{as}(CH$_2$) and v_s(CH$_2$) bands for NaDC are located at 2933 and 2861 cm^{-1}, respectively. But for [C$_{14}$mim]Br, v_{as}(CH$_2$) and v_s(CH$_2$) are located at 2918 and 2846 cm^{-1}, respectively. This indicated that the alkyl chains are highly ordered in [C$_{14}$mim]Br crystals and poorly ordered in NaDC crystals because of the big rigid steroid backbone. After the interaction between NaDC and [C$_{14}$mim]Br, the hydrocarbon chains still stack loosely compared with [C$_{14}$mim]Br crystals. Moreovre, Figure 8 a showed that for the spectrum of NaDC in solid, the double peaks of the carboxylate vibration at 1634 cm^{-1} (antisymmetric vibration, nas(COO)) and 1563 cm^{-1} (symmetric vibration, ns (COO)) can be found, indicating the ionic state.[24, 34] and the peak at 1070 cm^{-1} is in agreement with the stretching vibration of C-O bond

for NaDC. After the interaction between NaDC and [C$_{14}$mim]Br, the stretching vibration of carboxylate shifts to 1698 cm^{-1}, indicating the interaction between carboxylate groups and [C$_n$mim]$^+$. The wide peak at the range of 3350-3500 cm^{-1} is well-known for symmetric and antisymmetric O-H stretching modes, and it can be observed that the peak of O-H becomes so strong for NaDC/PBS hydrogel compared with NaDC crystals and it shifts from 3414 cm^{-1} to a higher frequency at 3442 cm^{-1} and the peak intensity also becomes weaker after the addition of [C$_n$mim]Br, indicating the formation of hydrogen bonds is hindered and the damage of the hydrogels induced by NaDC.
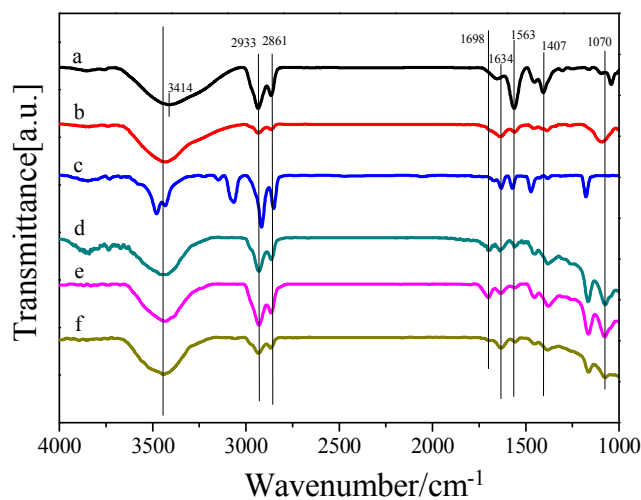
Figure 8 FT-IR patterns of (a) NaDC, (b) 50 mmol L^{-1} NaDC/100 mmol L^{-1} PBS, (c) [C$_{14}$mim]Br, (d) 5 mmol L^{-1} [C$_{14}$mim]Br/50 mmol L^{-1} NaDC/100 mmol L^{-1} PBS, (e) 5 mmol L^{-1} [C$_{12}$mimBr]/50 mmol L^{-1} NaDC/100 mmol L^{-1} PBS, (f) 5 mmol L^{-1} [C$_8$mimBr]/50 mmol L^{-1} NaDC/100 mmol L^{-1} PBS.

Furthermore, to get more detailed information about the hydrogels, powder X-ray diffraction (XRD) was performed [22, 28]. It can be seen from Figure 9 that for the NaDC or [C$_{14}$mim]Br

crystal, the peaks detected at a 2θ value of 10–22º which correspond to a short-range spacing might

be ascribed to the combination of several NaDC or [C$_{14}$mim]Br molecules through hydrophobic or

hydrogen bond interactions in the unit of the arrays. As is shown in Fig. 9 e and Fig. 9 f, after they

formed hydrogels in PBS buffer solutions, new peaks are detected at a 2θ value of 10–22º,

indicating that the interaction between NaDC and [C$_{14}$mim]Br. Moreover, as the concentration of

NaDC increases from 0 mmol L^{-1} to 5 mmol L^{-1}, the peaks at a 2θ value of 22–25º weaken,

demonstrating the structure of NaDC/PBS hydrogel was destroyed. The main peak for these

hydrogels are originated from NaH$_2$PO$_4$ and Na$_2$HPO$_4$ nanocrystals at a 2θ value of 22–70º.
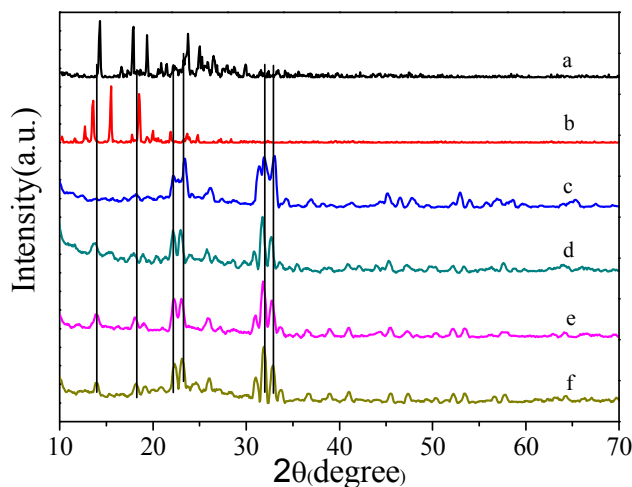
Figure 9 XRD patterns of   (a) [C$_{14}$mim]Br, (b) NaDC, (c) PBS, (d) 50 mmol L^{-1} NaDC/100 mmol

L^{-1} PBS, (e) 2 mmol L^{-1} [C$_{14}$mim]Br/50 mmol L^{-1} NaDC/100 mmol L^{-1} PBS, (f) 5 mmol L^{-1}

[C$_{14}$mim]Br/50 mmol L^{-1} NaDC/100 mmol L^{-1} PBS.

Different performance of [C$_2$mim]Br/NaDC/PBS mixed system

For [C$_2$mim]Br/NaDC/PBS system, its self-assemble behavior is very different from the others.

With the addition of [C$_2$mim]Br, it increased the mechanical strength of the mixed system gradually.

Moreover, when the concentration of [C$_2$mim]Br reached to 1250 mmol L^{-1}, it changed to two phase

state, that is, a spontaneous transition from transparent solution which was prepared immediately to

unstable gels and then to microcrystals can be achieved by ageing the gels at room temperature as

shown in Figure 10, that is, hydrogel of [C$_2$mim]Br/NaDC/PBS system consists of small fibers tens

of micrometers long, and these fibers further assemble into thick fiber bundles which are mostly by

a nucleation-growth process in solution and are not susceptible to a drying process [35]. Moreover,

under POM observation (Figure 11), it can be seen that all of these fibers possessed polarized

properties which indicated that the anisotropic properties of these fibers.

It is clearly indicated that this process is related to Ostwald ripening, in which smaller kinetically

favoured 'crystals' gradually aggregate into more thermodynamically favourable larger 'crystals'

[36]. Although Ostwald ripening is well known in crystallisation, the generation of crystals directly

from a gel is rare [37-40]. This can be inferred that donor-acceptor interactions drive complexation,

between the building blocks, and gelation is subsequently reinforced by hydrogen bond interactions.

This molecular recognition process occurs rapidly (minutes) leading to a homogeneous gel. Then,

over a period of hours, a kinetically slow process occurs in which the fibers aggregate laterally into

microcrystalline domains and the homogeneity of the gel is lost. During the process of crystallization,

an antiparallel dimer of DC$^-$ anion is considered as the fundamental building block for the wall of

such fibers. A schematic illustration of the interaction between DC$^-$ and [C$_2$mim]Br is given in

Scheme 2, which shows the possible molecular packing model of microcrystal structures.
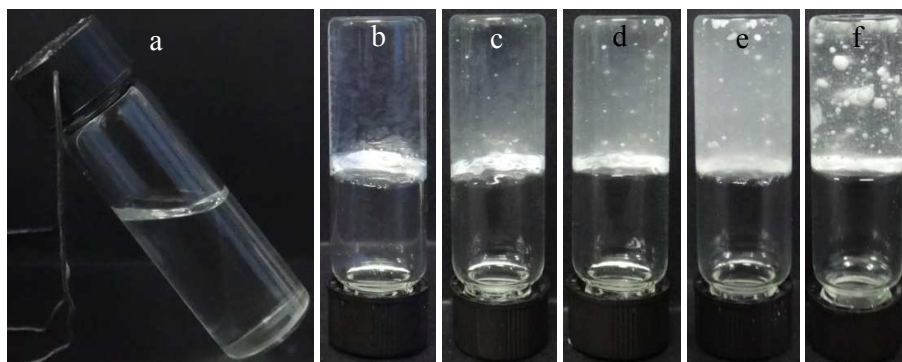
Figure 10 (a) Photograph of the transparent solution for the sample of 1500 mM [C$_2$mim]Br/50 mM NaDC in PBS buffer solution when the sample prepared immediately; Gel-crystal transition procedure with the sample at (b) 12 h, (c) 3 d, (d) 5 d, (e) 7 d and (f) 21 d.
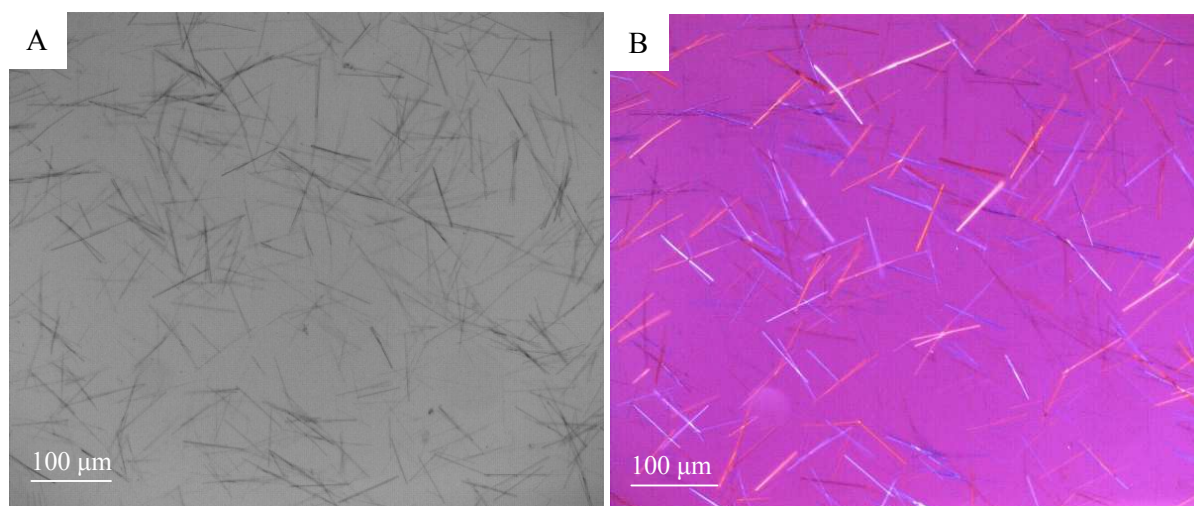
Figure 11 Optical microscope photo (A) and POM image (B) for 1500 mmol L^{-1} [C$_2$mim]Br/50 mmol L^{-1} NaDC/100 mmol L^{-1} PBS.
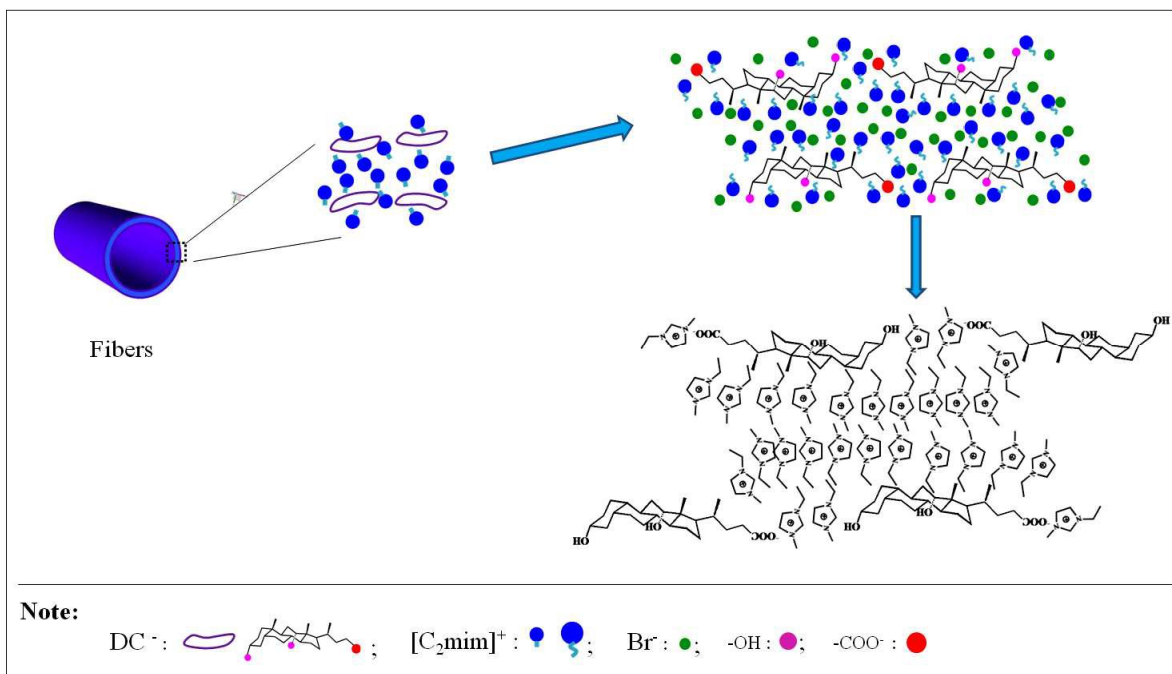
Scheme 2 Possible molecular packing model of microcrystal structures formed by NaDC and [C$_2$mim]Br.

Conclusion

In this paper, the interactions between [C$_n$mim]Br (n=2, 8, 12, 14) with NaDC in PBS buffer solution (pH = 7) were investigated systematically and the microstructures and properties of NaDC/C$_n$mimBr/PBS mixed systems were characterized using various techniques including TEM, FE-SEM, POM observations, FT-IR, XRD and rheological measurements. The results indicated that the long-chain imidazolium-based surfactants ([C$_n$mim]Br, n≥8) weakened the gel of NaDC and can change to sol, precipitate, two phase, solution and LLC phases, while C$_2$mimBr strengthened the gel behavior of NaDC and can form microcrystals. In the process of self assembly, electrostatic attraction, hydrophobic effect, and geometric packing all influence the phase behavior and the self-assembly structures of NaDC/[C$_n$mim]Br mixed systems.

Acknowledgement

References

[1] M. Jiang, A. Eisenberg, G. Liu and X. Zhang, Macromolecular self-assembly, Science Press, Beijing, 2006.

[2] A. Dolbecq, E. Dumas, C. Mayer and P. Mialane, *Chem. Rev.*, 2010, **110**, 6009–6048.

[3] A. Song and J. Hao, Curr. Opin. *Colloid Interface Sci.*, 2009, **14**, 94–102.

[4] J. Nanda and A. Banerjee, *Soft Matter*, 2012, **8**, 3380–3386.

[5] G.A. Silva, C. Czeisler, K.L. Niece, E. Beniash, D.A. Harrington, J.A. Kessler and S.I. Stupp, *Science*, 2004, **303**, 1352–1355.

[6] Y. Huang, Y. Yan, B. M. Smarsly, Z. Wei and C. F. J. Faul, *J. Mater. Chem.*, 2009, **19**, 2356–2362.

[7] G. Whitesides and B. Grzybowski, *Science*, 2002, **295**, 2418–2421.

[8] J. Moore and M. Kra, *Science*, 2008, **320**, 620–621.

[9] A. Gröschel, F. Schacher, H. Schmalz, O. Borisov, E. Zhulina, A. Walther, A. Müller, *Nat. commun.*, 2012**, 3,** 1−10.

[10] Y. Zakrevskyy, J. Stumpe and C. F. J. Faul, *Adv. Mater.*, 2006, **18**, 2133-2136.

[11] C. F. J. Faul, P. Krattiger, B. M. Smarsly and H. Wennemers, *J. Mater. Chem.*, 2008, **18**, 2962-2967.

[12] B. Jing, X. Chen, Y. Zhao, X. Wang, F. Ma and X. Yue, *J. Mater. Chem.*, 2009, **19**, 2037–2042.

[13] Z. Wang, C. J. Medforth and J. A. Shelnutt, *J. Am. Chem. Soc.*, 2004, **126**, 15954-15955.

[14] T. Zhang, C. Spitz, M. Antonietti, and C. F. J. Faul, *Chem. Eur. J.*, 2005, **11**, 1001–1009.

[15] Y. Gong, Q. Hu, N. Cheng, T. Wang, W. Xu, Y. Bi and L. Yu, *J. Mater. Chem. C*, 2015, **3**, 3273-3279.

[16] B. Dong, N. Li, L. Zheng, L. Yu and T. Inoue, *Langmuir*, 2007, **23**, 4178-4182.

[17] T. Inoue, H. Ebina, B. Dong and L. Zheng, *J. Colloid and Interface Sci.*, 2007, **314**, 236-241.

[18] N. Li, S. Zhang, L. Zheng, B. Dong, X. Li and L. Yu , *Phys. Chem. Chem. Phys.*, 2008, **10**, 4375-4377.

[19] F. Le. Dévédec, D. Fuentealba, S. Strandman, C. Bohne and X. Zhu, *Langmuir*, 2012, **28**, 13431−13440.

[20] F. He, G. Xu, J. Pang, T. Han, T. Liu and X Yang, *Luminescence*, 2012, **27**, 4−10.

[21] S. Song, L. Feng, A. Song and J Hao, *J. Phys. Chem. B*, 2012, **116**, 12850−12856.

[22] X. Sun, X. Xin, N. Tang, L. Guo, L. Wang, and G. Xu, *J. Phys. Chem. B*, 2014, **118**, 824-832.

[23] Y. Wang, X. Xin, W. Li, C. Jia, L. Wang, J. Shen and G. Xu, *J Colloid Interf Sci.*, 2014, **431**, 82-89.

[24] Y. Zhang, X. Xin, J. Shen, W. Tang, Y. Ren and L. Wang, *RSC Advances*, 2014, **4**, 62262-62271.

[25] M. C. di Gregorio, N. V. Pavel, A. Jover, F. Meijide, J. V,zquez Tato, V. H. Soto Tellini, A. Alfaro Vargas, O. Regev, Y. Kasavi, K. Schillén and K. L. Galantini, *Phys. Chem. Chem. Phys.*, 2013, **15**, 7560.

[26] LA Estroff, AD Hamilton, *Chem. Rev.*, 2004, **104**, 1201–1217.

[27] S. Song, R. Dong, D. Wang, A. Song, J. Hao, *soft Matter*, 2013, **9**, 4209-4218.

[28] L. Wang, X. Xin, M. Yang, X. Ma, J. Shen, Z. Song, S. Yuan, *Colloids Surf. A*, 2015, **483**, 112-120.

[29] X. Xu, Y. Jin, Y. Liu, X. Zhang and R. Zhuo, *Colloid and Surfaces B-Biointerfaces*, 2010, **81,** 329-335.

[30] K. Ouchi, C. L. Colyer, M. Sebaiy, J. Zhou, T. Maeda, H. Nakazumi, M. Shibukawa and S. Saito, *Analytical Chem.*, 2015, **87**, 1933-1940.

[31] L. Liu, L. Zhang, T. Wang and M. Liu, *Phys. Chem. Chem. Phys.*, 2013, **15**, 6243-6249.

[32] X. Cheng, Y. Peng, C. Gao, Y. Yan and J. Huang, *Colloids Surf. A*, 2013, **422**, 10–18.

[33] J. Shen, G. Xu, X. Xin, L. Wang, Z. Song, H. Zhang, L. Tong and Z. Yang, *RSC Adv.*, 2015, **5**, 40173–40182.

[34] H.Wang, S. Song, J. Hao, A. Song, *Chem. Eur. J.* 2015, **21**, 12194-12201.

[35] P. Zhu, X. Yan, Y. Su, Y. Yang, and J. Li, *Chem. Eur. J.*, 2010, **16**, 3176-3183.

[36] J. R. Moffat and D. K. Smith, *Chem. Commun.*, 2008, **19**, 2248-2250.

[37] O. Lebel, M. E. Perron, T. Maris, S. F. Zalzal, A. Nanci and J. D. Wuest, *Chem. Mater.*, 2006, **18**, 3616-3626.

[38] P. Terech, N. M. Sangeetha and U. Maitra, *J. Phys. Chem. B*, 2006, **110**, 15224-15233.

[39] D. K. Kumar, D. A. Jose, A. Das and P. Dastidar, *Chem. Commun.*, 2005, **119**, 4059-4061.

[40] D. Rizkov, J. Gun, O. Lev, R. Sicsic and A. Melman, *Langmuir*, 2005, **21**, 12130-12138.

Tailoring Self-assembly Behavior of Biological Surfactant By Imidazolium-based Surfactants with Different Length of Hydrophobic Alkyl Tails

Zhaohua Song , Xia Xin[*], Jinglin Shen, Han Zhang, Shubin Wang, Yanzhao Yang [*]
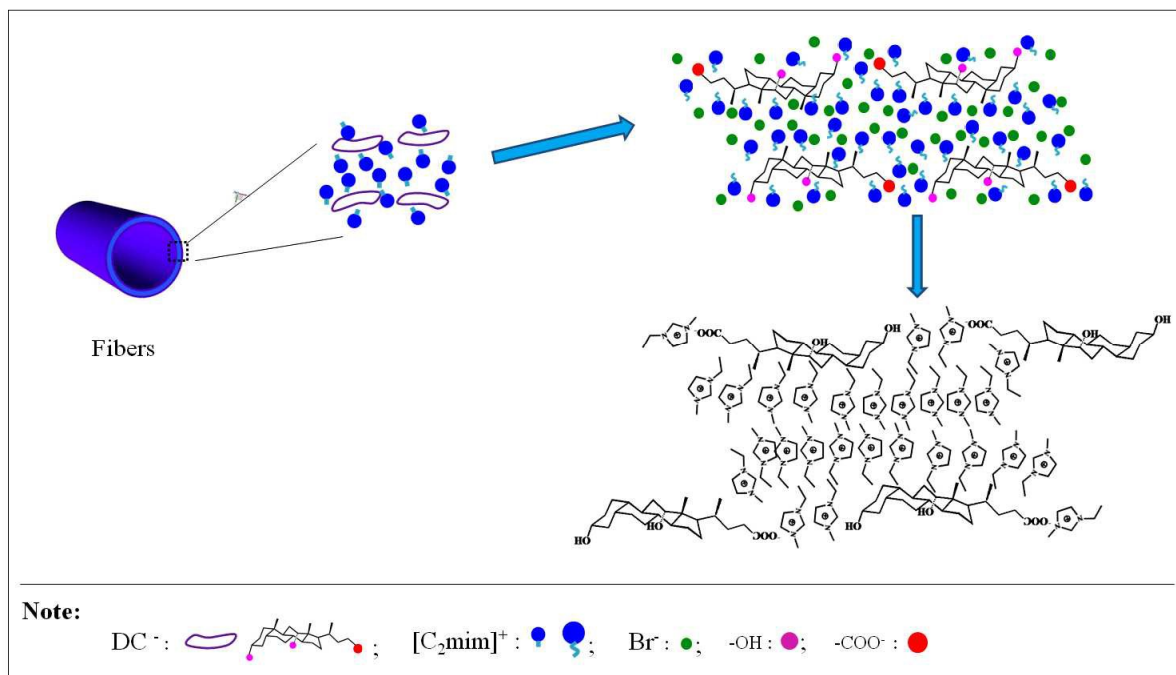
Possible molecular packing model of microcrystal structures formed by NaDC and [C$_2$mim]Br.

[*]Author to whom correspondence should be addressed, E-mail: xinx@sdu.edu.cn.

Phone: +86-531-88363597. Fax: +86-531-88361008

[*]Author to whom correspondence should be addressed, E-mail: yzhyang@sdu.edu.cn.

Phone: +86-531-88362988. Fax: +86-531-88361008